JGR Atmospheres

RESEARCH ARTICLE
10.1029/2023JD040228

Analyzing the Land Surface Temperature Response to Urban Morphological Changes: A Case Study of the Chengdu–Chongqing Urban Agglomeration

Yuhang Tian[1,2], Zhenghui Xie[1,2], Jinbo Xie[1], Binghao Jia[1], Si Chen[3], Peihua Qin[1], Ruichao Li[1], Longhuan Wang[1], Heng Yan[1,2], Yanbin You[1,2], and Bin Liu[4]

[1]State Key Laboratory of Numerical Modeling for Atmospheric Sciences and Geophysical Fluid Dynamics, Institute of Atmospheric Physics, Chinese Academy of Sciences, Beijing, China, [2]College of Earth and Planetary Sciences, University of Chinese Academy of Sciences, Beijing, China, [3]Research Institute, Qianhai Reinsurance Company Ltd., Shenzhen, China, [4]School of Software Engineering, Chengdu University of Information Technology, Chengdu, China

Abstract Urban morphological change impacts the land surface temperature (LST) through modifying the net radiation, convective heat transfer, evapotranspiration, and heat storage on the ground. It is essential to quantify the contributions of these physical changes on LST changes. In this work, we conduct simulations using a weather research and forecasting model for the Chengdu–Chongqing urban agglomeration to identify causes of LST changes due to urban morphological changes through different morphological parameters: the aspect ratio, building plan area fraction, and average building height. A new method is proposed and used to quantify the contribution of these physical changes on LST changes. The results show as the aspect ratio increases, an increase of the average LST is induced by variations in radiation, and daytime cooling and nighttime warming are induced by variations in heat storage. There is warming associated with an increase in the building plan area fraction, which is mostly caused by a decrease in the efficiency of the long-wave radiant heat emitted from the surface to the atmosphere. We also find that an increase in the average building height enhance the efficiency of convective heat transfer, which results in cooling. These results are important for the management of urban thermal environments.

Plain Language Summary Previous studies of the effects of urban morphological changes on the land surface temperature rarely quantified the contributions of different physical changes, including changes of the net radiation, convective heat transfer, evapotranspiration, and heat storage on the ground. Consequently, it is not clear which processes dominate the temperature changes. According to our analysis, which is based on simulations using a weather research and forecasting model, we found that an increase of the aspect ratio increases the radiation absorbed by urban surfaces, leading to an increase in the average temperature. As the aspect ratio increases, daytime cooling and nighttime warming result due to variations in heat storage. An increase of the building plan area fraction weakens the efficiency of the long-wave radiant heat emitted from the surface to the atmosphere, which leads to warming. We also find that there is cooling associated with an increase in the average building height, which is mostly induced by an increase in the efficiency of convective heat transfer. These results are important to understanding and design heat mitigation strategies.

Key Points:

- Land surface temperature response to urban morphological changes is attributed to different physical changes
- As the street aspect ratio increases, heat storage dominates the cooling effect during the daytime and the warming effect at nighttime
- The building area fraction affects the surface temperature mainly by changing the amount of long-wave radiation emitted by the surface

Supporting Information:

Supporting Information may be found in the online version of this article.

Correspondence to:

Z. Xie,
zxie@lasg.iap.ac.cn

Citation:

Tian, Y., Xie, Z., Xie, J., Jia, B., Chen, S., Qin, P., et al. (2024). Analyzing the land surface temperature response to urban morphological changes: A case study of the Chengdu–Chongqing urban agglomeration. *Journal of Geophysical Research: Atmospheres*, *129*, e2023JD040228. https://doi.org/10.1029/2023JD040228

Received 15 OCT 2023
Accepted 17 JAN 2024

1. Introduction

With the development of society and economy, the population in many developing countries is rapidly increasing in cities. Currently, the proportion of the global urban area in terms of total land area has reached 3% (Y. Zhou et al., 2015), and more than 50% of the global population lives in urban areas, which is expected to reach 6.7 billion by 2050 (United Nations, 2019). Such rapid urbanization seems to have been accompanied by land use and land cover changes, which potentially affect local and/or regional climates. This effect leads to an increase in the land surface temperature (LST) in urban areas, which strengthens the urban heat island effect (Broadbent et al., 2020; Krayenhoff et al., 2018). In addition, the urban morphology has a significant impact on urban microclimates (Lai et al., 2019), such as LST (Monaghan et al., 2014), urban heat islands (Kusaka, Chen, et al., 2004), extreme precipitation in urban areas (Li et al., 2013), and the boundary layer structure (Salamanca et al., 2011). The LST is a key variable of the urban thermal environment and has been applied as a thermal environment indicator in many studies (Chen et al., 2022; Khan et al., 2023; Mohammed et al., 2021; Peng et al., 2016; Yang

et al., 2019, 2021). Urban morphological changes affect the LST through physical changes including changes of net radiation, convective heat transfer, evapotranspiration, heat storage and other processes (Kim et al., 2021; Li, Zhang, et al., 2020; Nazarian & Kleissl, 2015; Yang & Li, 2015). Therefore, understanding the physical mechanism(s) of the impact of urban morphological changes on urban water and energy balances is very important toward disaster management.

The LST is greatly affected by urban morphological changes, including the aspect ratio, the building plan area fraction, and the average building height. R. Zhou et al. (2009) conducted sensitivity experiments on the aspect ratio with a boundary layer model by incorporating an urban canopy model and found that an increase of the aspect ratio will lead to daytime cooling and nighttime warming. Yang et al. (2017) also found the same phenomenon and point out that this is explained by an intensified heat storage capacity and a reduced solar radiation gain of urban surfaces. Kim et al. (2021) surmised that variations in the LST are explainable through changes in the upward sensible heat flux, because changes of the sensible heat flux are similar to changes of the LST. Hang and Chen (2022) suggested that an increase in the aspect ratio results in reduced convective ventilation and increased radiation trapping. It should be noted that these studies confused the roles of aspect ratio and the building height, and the impact of building height changes on the LST is consistent with the impact of aspect ratio changes. Guo et al. (2016) pointed out that the building plan fraction is the most important urban morphological parameter affecting local-scale LST. Many researchers have also pointed out that urban areas warm with an increase of the building plan area fraction (Lai et al., 2021; Lan & Zhan, 2017). However, these studies mentioned above focused merely on the heat fluxes, and did not quantify the contributions of various physical changes to the LST changes. It is not clear to what extent these different temperature changes caused by physical changes offset each other and which dominate changes on the LST (Li, Schubert, et al., 2020). Therefore, it is important to quantify the contributions of these different effects to changes in the LST accurately. It improves our understanding of the impacts of urban morphological changes on urban thermal environments. Such understanding is also important for policy makers and planners, because it can inform the design of warming mitigation strategies.

The two-resistance mechanism (TRM) method is commonly used for decomposing changes in the LST into contributions from net radiation; aerodynamic resistance, which controls the efficiency of convecting surface heat to the lower atmosphere; surface resistance, which controls evaporative cooling; heat storage; and anthropogenic heat flux (Rigden & Li, 2017). Liao et al. (2018) researched the mechanism of LST response to deforestation with the TRM method. Li and Zhang (2021) also identified the causes of the urban heat island effect with the TRM method. However, we find here that there is a significant difference between the emitted long-wave radiation calculated by the TRM method and that calculated using simulations of urban areas. Combined with the study of Kusaka et al. (2001), we find that the long-wave radiation emitted in urban areas is done so by multiple surfaces (e.g., roofs, walls, and streets) rather than being emitted by a single surface. Therefore, we define the equivalent surface emissivity to provide a surface energy balance closure relation and control the emitted long-wave radiation. The new method was named as the emissivity-two-resistance mechanism (ETRM) method and applied to quantify the contributions.

In this paper, we analyze the impact of three parameters-the aspect ratio (hw), building plan area fraction (lp), and average building height (h) on the LST of the Chengdu–Chongqing urban agglomeration (CCUA) using a weather research and forecasting (WRF) model and quantify contributions of physical changes to the LST changes. The ETRM method is used to determine the dominant processes affecting the LST, as caused by urban morphological changes. The paper is organized as follows: in Section 2, we describe the experiment design and method used in this study. Section 3 presents the results, and we conclude in Section 4.

2. Experiment Design and Method

2.1. Model Configuration

We used the WRF model with the advanced dynamic solver version 4.1.2 (Skamarock et al., 2019). The WRF model is developed by the NCEP and NCAR; it is a commonly used mesoscale numerical model and has been widely employed in simulations of urban meteorological environments (Deng et al., 2022; Grimmond et al., 2010; Millstein & Menon, 2011; Sun et al., 2021; Susca et al., 2011). This WRF model provides multiple physical parameterization options and we referred to Chen et al. (2022) when selecting the parameterization schemes. The main physical schemes for the model selection are the Thompson scheme (Thompson et al., 2008), Kain–Fritsch cumulus parameterization (Kain, 2004), the RRTM scheme (Mlawer et al., 1997), the Dudhia scheme (Dudhia, 1989),

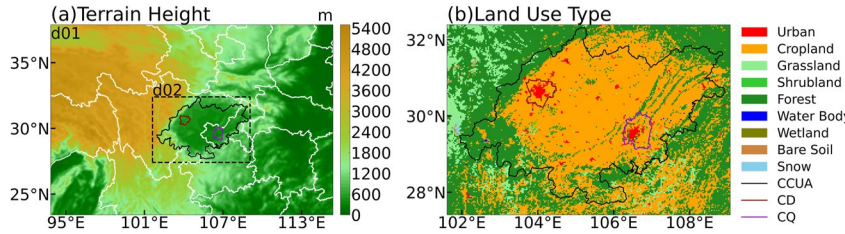

Figure 1. (a) Location and terrain height (m) of two nested domains. (b) The land use types of domain 2. The black line indicates the range of the Chengdu–Chongqing urban agglomeration (CCUA), the crimson line indicates the main urban area of Chengdu (CD), and the purple line indicates the main urban area of Chongqing (CQ).

the Mesoscale Model version 5 Monin–Obukhov surface layer scheme (Jiménez et al., 2012), the BouLac PBL (Hong et al., 2006), and the Noah land surface model (Chen & Dudhia, 2001). We utilized a single-layer urban canopy model in the WRF for urban canopy parameterization, where the single-layer urban canopy model can obtain the energy and momentum exchange between the atmosphere and urban surfaces and estimate heat fluxes and surface temperatures from walls, streets, and roofs (Kusaka & Kimura, 2004; Kusaka et al., 2001).

The study area is the Chengdu–Chongqing urban agglomeration, which is located in a mountainous area of southwest China. There are two megacities, Chengdu (CD) and Chongqing (CQ), which have a high city density and urbanization level (Wang et al., 2015). We set up two-layer nested domains in the horizontal direction (Figure 1a), with resolutions of 9 and 3 km, respectively, and we divided the atmosphere into 30 vertical layers. The simulation periods were set from 01 May to 01 September (summer) and from 01 November to 01 March of the next year (winter) over 2017, 2018, 2019, 2020, and 2021, with the first month considered as the spin-up period. The time steps for two domains were 15 s, and 3 s. The initial and lateral boundary conditions for the large-scale atmospheric fields were derived from the National Centers for Environmental Prediction (NCEP) Global Final Analysis (FNL), with a spatial resolution of $1° \times 1°$ and a time interval of 6 hr (https://doi.org/10.5065/D6M043C6). Similar to Chen et al. (2022), we obtained the 1 km spatial resolution fusion land cover data in 2020 (Figure 1b) from the Resource and Environment Science and Data Center (Xu et al., 2018; https://doi.org/10.12078/2018070201) and reclassified the land use and land cover data into 24 categories according to the International Geosphere-Biosphere Project classification scheme of the USGS to meet the classification standard in the WRF model. Finally, results of the model simulations were output every 1 hr.

2.2. Calculating the LST in the WRF

In this subsection, we introduce the calculation of LST in the WRF. The single-layer urban canopy model was coupled with the Noah land surface model within the WRF models using a tile approach (Chen et al., 2011). When the single-layer urban canopy model is used, the urban grids are divided into impervious and natural surfaces. In the Noah land surface model, the natural surface of the grid is assumed to represent a mosaic consisting of croplands and grasslands, and the natural LST is calculated to close the surface energy balance. In the WRF, the Noah land surface model is called to calculate the LST and other variables of the natural surfaces. Then the single-layer urban canopy model is called to calculate these variables for the impervious surfaces. The fractions of the impervious and natural surfaces are based on the impervious surface coverage (f_{urb}) in the urban parameter table. The LST (T_{s}) for the entire grid is calculated as a weighted average of the impervious and natural surface temperatures:

$$T_{\mathrm{s}} = f_{\mathrm{urb}} \times T_{\mathrm{s,impervious}} + (1 - f_{\mathrm{urb}}) \times T_{\mathrm{s,natural}}, \tag{1}$$

where, $T_{\mathrm{s,\ impervious}}$ represents the LST for impervious surfaces, $T_{\mathrm{s,\ natural}}$ represents the LST for natural surfaces. The equation of $T_{\mathrm{s,\ impervious}}$ is defined as follows:

$$T_{\mathrm{s,impervious}} = T_{\mathrm{a}} + \frac{H_{\mathrm{impervious}}}{\rho C_{\mathrm{p}} C_{\mathrm{h}} U_{\mathrm{a}}}, \tag{2}$$

where, T_{a} represents the air temperature at the lowest model level, ρ is the air density, C_{p} is the specific heat at constant pressure, C_{h} is the bulk transfer coefficient for heat, U_{a} is the wind speed at the first level of the atmospheric model. And $H_{\mathrm{impervious}}$ represents the sensible heat flux, is an area-weighted average of the sensible heat fluxes from the different surfaces. The equation of $H_{\mathrm{impervious}}$ is defined as follows:

$$H_{\mathrm{impervious}} = F_{\mathrm{roof}} \times H_{\mathrm{s,roof}} + F_{\mathrm{street}} \times H_{\mathrm{s,street}} + F_{\mathrm{wall}} \times H_{\mathrm{s,wall}}, \tag{3}$$

Table 1
Parameter Values Considered in Sensitivity Experiments

Experiments	hw(−)	lp(−)	h(m)	f_{urb} (−)
Exp0	Urban canopy parameters data set for 60 Chinese cities			FROM-GLC10
Exp1	0.5	0.33	20	0.9
Exp2	1.0	0.33	20	0.9
Exp3	0.5	0.5	20	0.9
Exp4	0.5	0.33	40	0.9

where, $H_{s,\ roof}$ represent the sensible heat flux of roofs, $H_{s,\ street}$ represent the sensible heat flux of streets, $H_{s,\ wall}$ represent the sensible heat flux of walls, F_{roof} is the ratio of roof area to urban area, F_{street} is the ratio of street area to urban area, and F_{wall} is the ratio of wall area to urban area.

Different to natural surfaces, impervious surfaces representing the urban canopy should be treated as three-dimensional urban geometries (e.g., roofs, walls, and streets). According to Kanda et al. (2007), the LST for impervious surfaces can be estimated by using Monin–Obukhov similarity theory in the single-layer urban canopy model (see Equations 2 and 3).

2.3. Experimental Design

To examine the effects of urban morphological changes (aspect ratio (hw), building plan area fraction (lp), and average building height (h)) on the LST, we conducted five experiments (Table 1). The Exp0 was conducted to verify the credibility of the model. In this experiment, we used an urban canopy parameter data set consisting of 60 Chinese cities (Sun et al., 2021) to describe the urban structures, and the FROM-GLC10 data set (Gong et al., 2019) to describe the impervious surfaces. And the other four experiments are sensitivity experiments based on different values of the urban morphological parameters (Exp1, Exp2, Exp3, and Exp4). The difference between Exp2 and Exp1 (Exp2–Exp1) was taken as a proxy of increasing the aspect ratio; Exp3–Exp1 represents the effect of increasing the building plan area fraction; and Exp4–Exp1 represents the effect of increasing the average building height. The values of the urban morphological parameters were selected according to the study of Stewart and Oke (2012). In addition, we set the impervious surface coverage (f_{urb}) to 0.9, which is the default value in the WRF model, to make the signals in the urban grid more obvious and eliminate errors caused by differences in the impervious surface coverage.

The three urban morphological parameters have clear and intuitive physical meanings in the model. First, the aspect ratio (hw) describes the geometry of a "street canyon", where a higher value indicates a deeper canyon. Many researchers have found that the aspect ratio greatly affects the surface thermal environment (Marciotto et al., 2010; Yang et al., 2017). Second, the building plan area fraction (lp) is the proportion of building area to the total urban area; it is represented by the normalized building width (r = lp) in the single-layer urban canopy model, where a higher value indicates a larger building area. In addition, the normalized street width is uniquely determined by r ($w = 1–r$), so the building plan area fraction also represents the proportion of street area to the total urban area, where a higher value indicates a smaller street area. Lastly, h is the average building height, and we separate the effect of average building height changes from that of aspect ratio changes.

Interestingly, only the aspect ratio and building plan area fraction are involved when calculating the radiation, and the average building height does not have a direct affect (Text S1 in Supporting Information S1). According to the description of radiation in urban areas in Kusaka et al. (2001), an increase of the aspect ratio will increase the amount of solar radiation flux absorbed by the urban area. In addition, diffuse solar radiation and atmospheric long-wave radiation absorbed by a street canyon are only related to the aspect ratio instead of the average building height (Text S1 in Supporting Information S1). However, many researchers did not distinguish the effects caused by changes in the average building height and aspect ratio (Hang & Chen, 2022; Kim et al., 2021; Yang et al., 2017; R. Zhou et al., 2009). So, it is important to separate the changes caused by the average building height from those caused by the aspect ratio.

We are unable to adjust the aspect ratio and building plan area fraction directly in the WRF model, so it is necessary to convert them to parameters that can be changed. The corresponding equations are as follows:

$$\mathrm{sw} = \frac{\mathrm{h}}{\mathrm{hw}}, \tag{4}$$

$$\mathrm{bw} = \frac{\mathrm{sw} \times \mathrm{lp}}{1 - \mathrm{lp}}, \tag{5}$$

where sw is the street width and bw is the building width, which are listed in the urban parameter table.

When we adjusted the street width and building width, these changes do not directly cause physical changes; however, indirect physical changes arose by changing the aspect ratio and building plan area fraction. It should be noted that when we adjusted the street width to change the aspect ratio, the building plan area fraction changed accordingly. To offset the impact of street width changes on the building plan area fraction, we adjusted the building width accordingly. Similarly, when we adjusted the average building height, the aspect ratio and building plan area fraction were impacted. To offset these impacts, we adjusted the street width to compensate for the corresponding changes in the aspect ratio and similarly changed the building width to compensate for changes in the building plan area fraction. So, in our experiment, the changes in street width and building width do not cause additional physical changes in the urban LST.

2.4. ETRM Method

In order to decompose the differences of the LST into contributions from different physical changes we used the TRM method, which has been widely used to attribute changes on LST to various factors (Liao et al., 2018, 2020; Rigden & Li, 2017). However, when we utilized it in urban areas, we found that there was a large deviation between the emitted long-wave radiation ($L_s\uparrow$) calculated by the TRM method and the simulated $L_s\uparrow$, which is caused by the special structure of the urban environment (Text S2 in Supporting Information S1). Therefore, we propose an alternative approach for attributing changes in the LST by controlling the emitted long-wave radiation with the equivalent surface emissivity (ε_s), which we refer to as the ETRM method. We argue that from a land surface modeling perspective and when land–atmosphere feedback is not considered (an assumption also made in the TRM method), ε_s can be viewed as an input. It should be noted that the absorptivity of the atmospheric long-wave radiation absorbed by the surface and the emissivity of the long-wave radiation emitted by the surface are different concepts. Although in most cases, they are equal and represented by the emissivity, we find that this approach does not hold in urban areas (Text S2 in Supporting Information S1). The prerequisite for absorptivity and emissivity to be equal is a single surface with a uniform temperature distribution. In urban areas, however, there are multiple surfaces with different temperatures (e.g., roofs, walls, and streets). To distinguish them, we refer to ε as the absorptivity and ε_s as the equivalent surface emissivity.

In addition, we also considered the case when the absorptivity is equal to the equivalent surface emissivity (Text S3 in Supporting Information S1). We found that the ETRM method can also be applied to this case of $\varepsilon = \varepsilon_s$ and distinguish the changes in the atmospheric long-wave radiation absorbed by the surface and the long-wave radiation emitted by surface. Under this condition, the ETRM method is the same as the method of Liao et al. (2020). The detailed derivations are presented in the Text S3 in Supporting Information S1. Here only the final results are reproduced:

$$\Delta T_s \approx \frac{\partial \mathrm{T_s}}{\partial \mathrm{S_n}} \times \Delta S_\mathrm{n} + \frac{\partial \mathrm{T_s}}{\partial \mathrm{L_n^*}} \times \Delta L_\mathrm{n}^* + \frac{\partial \mathrm{T_s}}{\partial \varepsilon_s} \times \Delta \varepsilon_s \frac{\partial \mathrm{T_s}}{\partial \mathrm{r_a}} \times \Delta r_\mathrm{a} + \frac{\partial \mathrm{T_s}}{\partial \mathrm{r_s}} \times \Delta r_\mathrm{s} + \frac{\partial \mathrm{T_s}}{\partial \mathrm{Q_s}} \times \Delta Q_\mathrm{s}. \tag{6}$$

The terms on the right-hand side of Equation 6 represent the impact of changes in the net solar radiation ($\frac{\partial \mathrm{T_s}}{\partial \mathrm{S_n}} \times \Delta S_\mathrm{n}$; where S_n is the net solar radiation), the atmospheric long-wave radiation absorbed by the surface ($\frac{\partial \mathrm{T_s}}{\partial \mathrm{L_n^*}} \times \Delta L_\mathrm{n}^*$; where L_n^* is the atmospheric long-wave radiation absorbed by surface), the efficiency of the long-wave radiant heat emitted from the surface to the atmosphere ($\frac{\partial \mathrm{T_s}}{\partial \varepsilon_s} \times \Delta \varepsilon_s$; where ε_s is the equivalent surface emissivity), the efficiency of convecting surface heat to the lower atmosphere ($\frac{\partial \mathrm{T_s}}{\partial \mathrm{r_a}} \times \Delta r_\mathrm{a}$; where r_a is the aerodynamic resistance), evaporative cooling ($\frac{\partial \mathrm{T_s}}{\partial \mathrm{r_s}} \times \Delta r_\mathrm{s}$; where r_s is the surface resistance), and the heat storage ($\frac{\partial \mathrm{T_s}}{\partial \mathrm{Q_s}} \times \Delta Q_\mathrm{s}$; where Q_s is the heat storage) on the surface temperature. It should be noted that the long-wave radiant heat emitted by the surface to the atmosphere excludes atmospheric long-wave radiation reflected by the surface. In addition, anthropogenic heat (Q_ah) in the single-layer urban canopy model is determined according to the temporal profile, and as urban morphological changes do not lead to any Q_ah changes, we neglect this term in the simulations. At the same time, we also assume that urban morphological changes will not affect the background climate state above the mixing height; hence, ΔT_a is also omitted.

With the ETRM method, we can decompose ΔT_s caused by urban morphological changes into contributions from physical changes, where $\Delta T_s = T_{dis} - T_{ref}$ represents the temperature disturbance (where "dis" and "ref" indicate the disturbed and reference state, respectively, the selections of which are described Section 2.3), and optimize the ETRM method to reduce the errors between the calculated ΔT_s ($\Delta T_s{}^C$, calculated using Equation 6) and simulated ΔT_s ($\Delta T_s{}^M$) (Liao et al., 2018). Finally, we also made a comparison between the results obtained with the TRM method, based on Liao et al. (2020), and the ETRM method. We found that the main reason for the poor capture effect of the TRM method on LST changes is the inaccurate capture of the emitted long-wave radiation (Text S4 in Supporting Information S1).

2.5. Application of the ETRM Method

Based on the four simulations (Exp1, Exp2, Exp3, and Exp4), we searched for differences between them to obtain the impact of three urban morphological parameters (aspect ratio (hw), building plan area fraction (lp), and average building height (h)) on the LST. We decompose the changes on the LST into contributions from the net solar radiation (ΔS_n), the atmospheric long-wave radiation absorbed by the surface (ΔL_n), the equivalent surface emissivity ($\Delta \varepsilon_s$), the aerodynamic resistance (Δr_a), the surface resistance (Δr_s), and heat storage (ΔQ_s); these were quantified as the daily mean, daytime, and nighttime values during summer and winter. First, we attributed LST changes to contributions from different physical changes on the daily scale and then averaged the results for each period. We ignored any unstable changes of weather and meteorology caused by slight differences of the chaotic weather systems, and only focused on stable, average climate states. Second, we calculated the averages and standard deviations of these results for urban grids in the Chengdu–Chongqing urban agglomeration, Chengdu, and Chongqing. Lastly, we analyzed the three urban morphological parameters, as plotted in Figures 4–6, respectively. If the difference between the ΔT_s calculated using the summed contributions ($\Delta T_s{}^C$) and simulated ($\Delta T_s{}^M$) was small, we consider that the result is accurate.

3. Results

3.1. Evaluation

It is essential to ensure the credibility of modeled results. Due to the lack of LST data observed from ground stations, we used the near-real-time LST product data set of the China Meteorological Administration Land Data Assimilation System (CLDAS; http://data.cma.cn/data/cdcdetail/dataCode/NAFP_CLDAS2.0_NRT), which has a spatial resolution of 0.0625° × 0.0625° and a time interval of 1 hr (Han et al., 2015; Shi et al., 2008, 2011; Sun et al., 2017; Zhu et al., 2013), and the LST product data set of the land component of the fifth generation of European ReAnalysis (ERA5-Land; https://doi.org/10.24381/cds.e2161bac), which has a spatial resolution of 0.1° × 0.1° and a time interval of 1 hr (Muñoz Sabater, 2019). These data are used to verify the LST output from Exp0 (see in Table 1). The LSTs of CLDAS were derived from satellite observations from various sources and the CLM3.5, CoLM, and Noah-MP land surface models. These land surface models were driven by the CLDAS atmosphere forcing data. Similarly, the LSTs of ERA5-Land were derived from the European Center for Medium-Range Weather Forecasts (ECMWF) land surface model. And the land surface model was driven by atmospheric forcing data derived from the ERA5 near-surface meteorology state and flux fields. We noted that these land surface models are not coupled with an urban canopy model. Instead, they are used to calculate the urban grid in the same way as for natural surfaces by changing the land surface parameters, without considering the three-dimensional structure of the urban canyon and treating it as a simple surface (Dai et al., 2003; ECMWF, 2018; Li et al., 2017; Niu et al., 2011; Oleson et al., 2007). In other words, these land surface models lack consideration of walls and treat roofs and streets as one surface.

We evaluated the mean LST for daily mean, daytime and nighttime in summer and winter and mainly verified the correlation between the WRF simulations and these LST products (Figure 2). According to the hourly incoming shortwave radiation output from the WRF, we categorized all hours with positive incoming shortwave radiation as daytime, and those with zero shortwave radiation as nighttime (Huang et al., 2021). We then validated the LST time series. We first averaged the LST of the grids in Chengdu (CD) and Chongqing (CQ) (Figure 1b) to compare the time series produced by the WRF simulation with the CLDAS and ERA5-Land data sets, and then calculated the correlation coefficient between them. In Figure 2, it is clear that there is acceptable agreement between the WRF simulation and the two sets of reanalysis data, where all correlation coefficients are greater

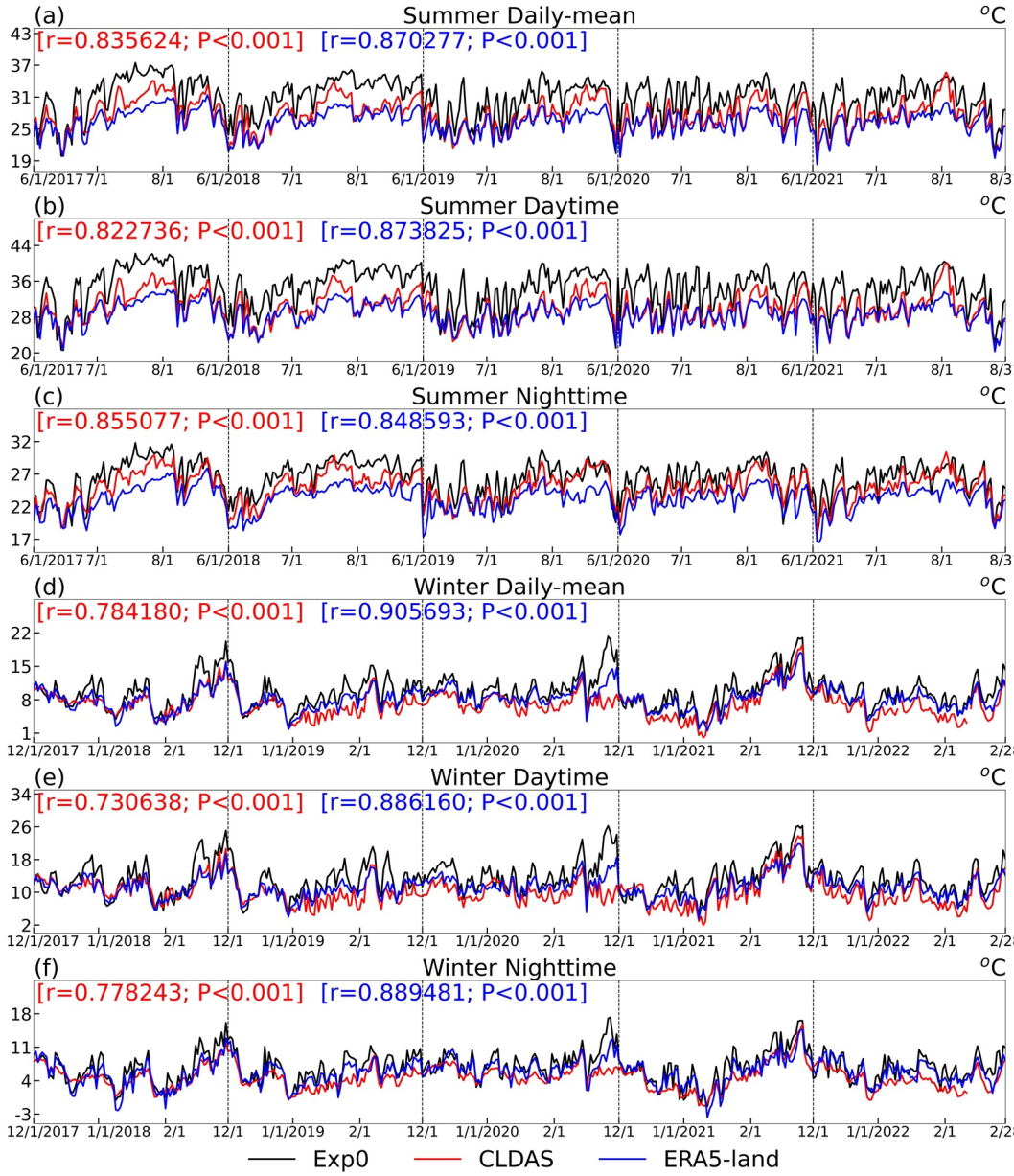

Figure 2. Comparison between the Exp0 (black curve), CLDAS (red curve), and ERA5-Land (blue curve) LSTs: (a) summer daily mean, (b) summer daytime, (c) summer nighttime, (d) winter daily mean, (e) winter daytime, and (f) winter nighttime in the grids of Chengdu (CD) and Chongqing (CQ).

than 0.73 and all confidence levels are above 99.9%. These show that the configuration of the model is reasonable. However, the simulations overestimate the LST compared with data from CLDAS and ERA5-Land. The lack of wall temperatures in LST products may be one of the sources of these deviations. In summer, the LST differences between the WRF simulation and CLDAS are smaller than between the WRF simulation and ERA5-Land. This may be because the LSTs of CLDAS are derived from satellite observations and the CLM3.5, CoLM, and Noah-MP land surface models in the study area, producing more accurate LSTs than ERA5-Land. Moreover, previous studies have reported similar differences, characteristic of the WRF model (Barlage et al., 2016; Chen et al., 2014; Grossman-Clarke et al., 2010; Li & Zhang, 2021; Salamanca et al., 2018; Sharma et al., 2016; Wang et al., 2020), with most overestimations occurring in the urban regions of the respective study areas. Since we are concerned with the changes in the LST caused by urban morphological changes, these systematic deviations can be offset by sensitivity experiments in the study area.

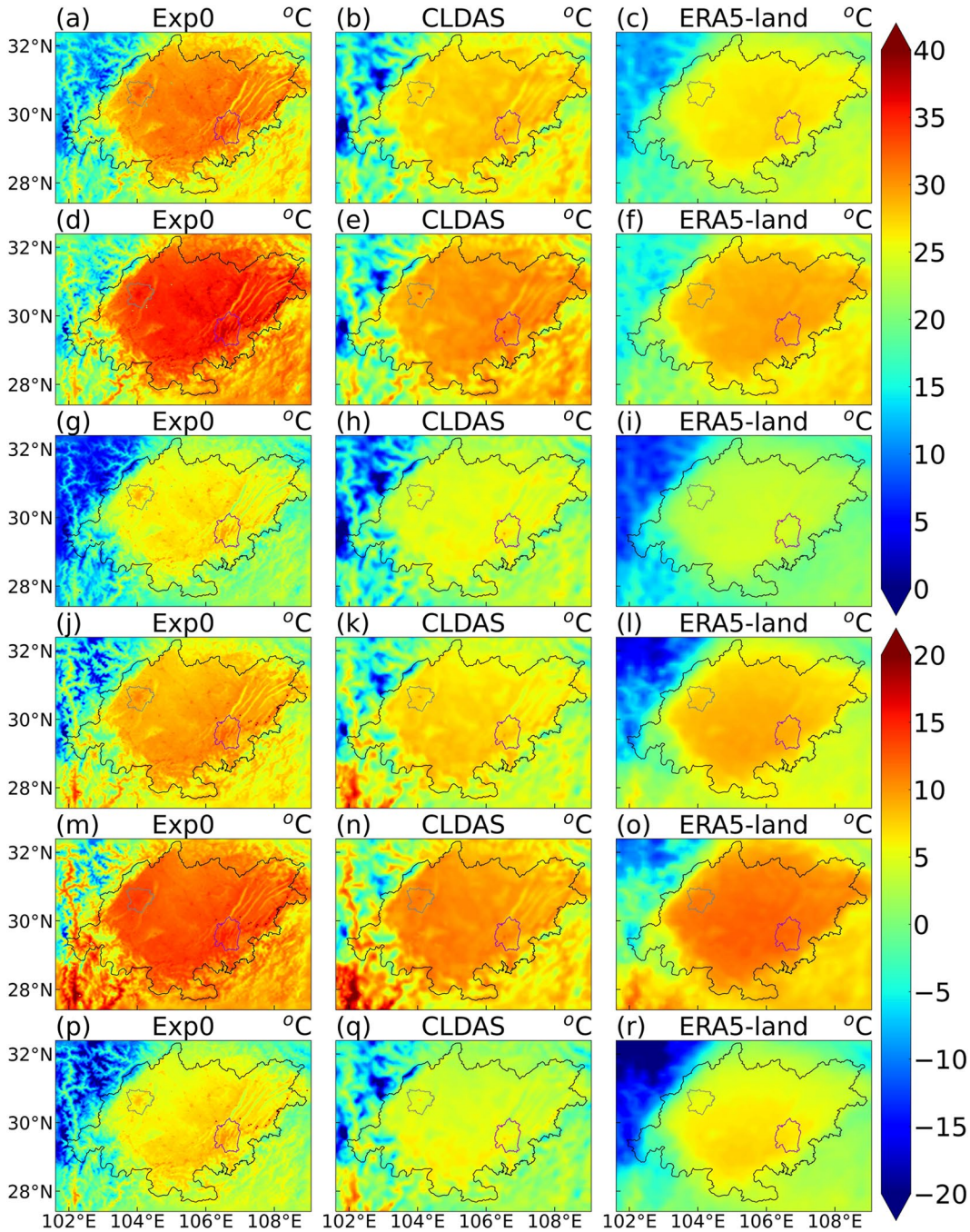

Figure 3. Spatial pattern of the LST from the Exp0, CLDAS data sets, and ERA5-Land data sets for: (a–c) summer daily mean, (d–f) summer daytime, (g–i) summer nighttime, (j–l) winter daily mean, (m–o) winter daytime, and (p–r) winter nighttime.

In addition to the time series comparison, we also compare the spatial pattern of the LST. To facilitate model evaluation, the simulated LSTs were averaged into daily mean, daytime, and nighttime values in the summers and winter of 2017–2021, and compared with their corresponding values obtained with the CLDAS and ERA5-Land data sets (Figure 3). It is shown that the simulation results successfully reproduce the spatial variability of the LST with reasonable fidelity, simulating low values in mountainous areas and high values in Sichuan Basin. In general, the simulations accurately capture both the time-varying and spatially varying climatological behavior during our simulated time period.

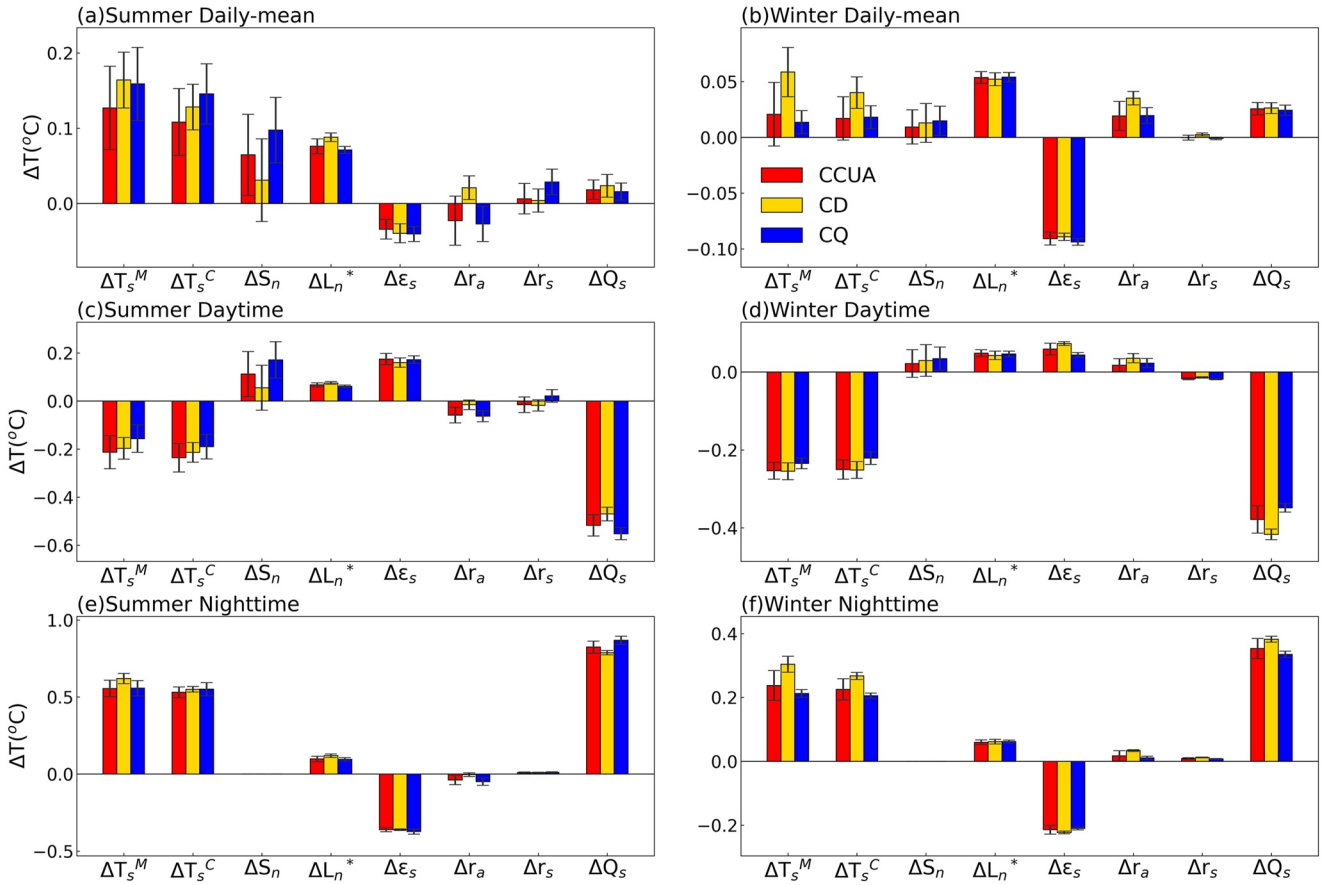

Figure 4. The ΔT_s caused by an increase in the aspect ratio (hw) and various attributing factors. (a–b) Results of the daily mean in summer and winter. (c–d) Results for the daytime in summer and winter. (e–f) Results for the nighttime in summer and winter. ΔT_s^M and ΔT_s^C represent the simulated ΔT_s and calculated ΔT_s using the summed contributions, respectively, and ΔS_n, ΔL_n^*, $\Delta \varepsilon_s$, Δr_a, Δr_s, and ΔQ_s represent different factors controlling the variations of ΔT_s (see the main text for definitions of these factors). Red, yellow, and blue bars represent results for the Chengdu–Chongqing urban agglomeration (CCUA), Chengdu (CD), and Chongqing (CQ), respectively.

3.2. Response of the LST to Urban Morphological Changes

3.2.1. Response of the LST to an Increase of Aspect Ratio

Figure 4 shows the simulated and calculated ΔT_s due to aspect ratio increases, where these results are based on the ETRM method. As the results of the Chengdu–Chongqing urban agglomeration, Chengdu, and Chongqing are very similar, hereafter we will only discuss the results for the Chengdu–Chongqing urban agglomeration. In summer, an increase in the aspect ratio causes the mean LST to increase by ~0.13°C. This is because of a change in the ground's capacity to absorb solar radiation and atmospheric long-wave radiation, and the change is caused by a decrease in the albedo and an increase in the absorptivity (Text S1 in Supporting Information S1). ΔS_n contributes ~0.06°C to the ΔT_s and ΔL_n contributes ~0.08°C (Figure 4a). It is important to note that the average building height does not change, so the increase of the aspect ratio directly enhances the radiation trapping effect. In addition, $\Delta \varepsilon_s$ contributes ~−0.03°C and ΔQ_s contributes ~0.02°C.

However, an increase in aspect ratio leads to a daytime cooling effect (~−0.21°C), although it increases the solar radiation absorbed by the urban surface during the daytime (contributes ~0.11°C; Figure 4c). We find that ΔQ_s contributes ~−0.52°C during the daytime in summer and the contributions of the other factors are less than that of ΔQ_s. During the nighttime in summer, the LST increases by ~0.56°C and ΔQ_s contributes ~0.82°C (Figure 4e). According to the study of Rigo and Parlow (2007), the land surface absorbs and stores energy from the atmosphere during the daytime and releases it at nighttime. It is known that the larger the aspect ratio, the greater the total surface area of the urban area, which makes the energy absorbed by the surface increase during the daytime, so that ΔQ_s plays a cooling role; meanwhile, heat is released during the nighttime, meaning ΔQ_s

plays a warming role at night (Yang et al., 2017). In addition, ΔL_n contributes a weak warming effect (~0.07°C in daytime; ~0.10°C in nighttime), because the increase of absorptivity makes the land absorb more atmospheric long-wave radiation.

The contribution of $\Delta\varepsilon_s$ is interesting, which provides a positive contribution (~0.17°C; Figure 4c) during the daytime and a negative contribution during the nighttime (~−0.36°C; Figure 4e). According to the study of Kusaka et al. (2001), the structure of the street canyons increases the area that emits long-wave radiation. This enhances the radiative heat dissipation, and the area that emits long-wave radiation increases with an increase of the aspect ratio. However, street canyons will reabsorb the emitted long-wave radiation and the area that reabsorbs long-wave radiation also increases with an increase of the aspect ratio (Text S1 in Supporting Information S1). For the nighttime and daily mean, the contribution of $\Delta\varepsilon_s$ is negative (Figures 4a, 4b, 4e and 4f), because the radiation heat dissipation increases rapidly with an increase of the aspect ratio. However, during the daytime, $\Delta\varepsilon_s$ causes a warming effect (Figures 4c and 4d), because the radiation reabsorbed by street canyons increases more than the radiation emitted by street canyons.

We also find that, during the daytime, the contributions of ΔS_n, ΔL_n, and $\Delta\varepsilon_s$ are positive, so that the radiation change caused by an increase in the aspect ratio provides a warming effect. However, Marciotto et al. (2010) points out that an increase of the aspect ratio will reduce the net surface radiation during the daytime, which seems to be contradicted by our study. However, they only considered their variables at 12:00 local time in their research, which only represents the radiation change at the time of maximum solar elevation angle. Instead, we used the average value of the variables during the daytime in our research, which represents the radiation change throughout the daytime. Therefore, although there are differences between Marciotto et al. (2010)'s and our research, our respective results are not contradictory. We surmised that changes in the solar elevation angle causes changes in the shadow effect of street canyons, affecting the surface net radiation. Therefore, the radiation changes at 12:00 local time, during the time with the weakest shadow effect, are different from the average radiation changes throughout the daytime. In addition, their research only simulated two typical days of the year, while we simulated summer and winter over 5 years, which may also lead to the difference between the results of Marciotto et al. (2010) and our research.

In winter, the aspect ratio increase has little effect on the LST. It is because the amount of absorbed solar radiation and absorbed atmospheric long-wave radiation in winter is much less than in summer (ΔS_n contributes ~0.01°C; ΔL_n contributes ~0.05°C; see Figure 4b). The contributions of $\Delta\varepsilon_s$, Δr_a, and ΔQ_s cannot be ignored, as $\Delta\varepsilon_s$ contributes ~−0.09°C, Δr_a contributes ~0.02°C, and ΔQ_s contributes ~0.03°C. During the daytime and nighttime, the results of ΔT_s in winter are similar to those in summer (Figures 4d–4f). Due to the weak contribution of ΔS_n, the daytime cooling effect in winter is stronger than in summer. In addition, the decrease of solar radiation also makes the contribution of ΔQ_s in winter weaker than in summer, where ΔQ_s contributes ~−0.38°C in daytime and ~0.35°C in nighttime.

3.2.2. Response of the LST to an Increase of the Building Plan Area Fraction

With an increase of the building plan area fraction, the ETRM method can still capture the LST changes (Figure 5), and, as in the previous section, here we only discuss the results obtained in the Chengdu–Chongqing urban agglomeration. The results show that an increase in building plan area fraction causes the mean LST to increase (~0.59°C in summer and ~0.20°C in winter), which affects the LST through adjusting the proportion of building area and street area to change the proportion of the effect caused by the street canyons in the urban areas. $\Delta\varepsilon_s$ provides the greatest contribution, which increases by ~0.63°C in summer and ~0.33°C in winter (Figures 5a and 5b). According to the analysis in the previous section, street canyons enhance the efficiency of the long-wave radiant heat emitted from the surface to the atmosphere, and we know that an increase of the building plan area fraction means a decrease in the area of street canyons (see Section 2.3); so, the efficiency of the long-wave radiant heat emitted from the surface to the atmosphere decreases and provides a significant positive contribution. In addition, the street canyons decrease the albedo and increase the absorptivity, and a larger building plan area fraction decreases the area of street canyons; so, the increase of the building plan area fraction increases the albedo, which leads to a cooling effect of ΔS_n, and also decreases the absorptivity, which lead to a cooling effect of ΔL_n. Street canyons also increase the roughness of the urban surface and increase the area of evaporation and heat absorption and release, and a larger building plan area fraction decreases the area of street canyons. As such, with an increase of the building plan area fraction, the roughness decreases, leading to positive contributions of Δr_a and Δr_s. The increase of the building plan area fraction also leads to a positive contribution of ΔQ_s in summer

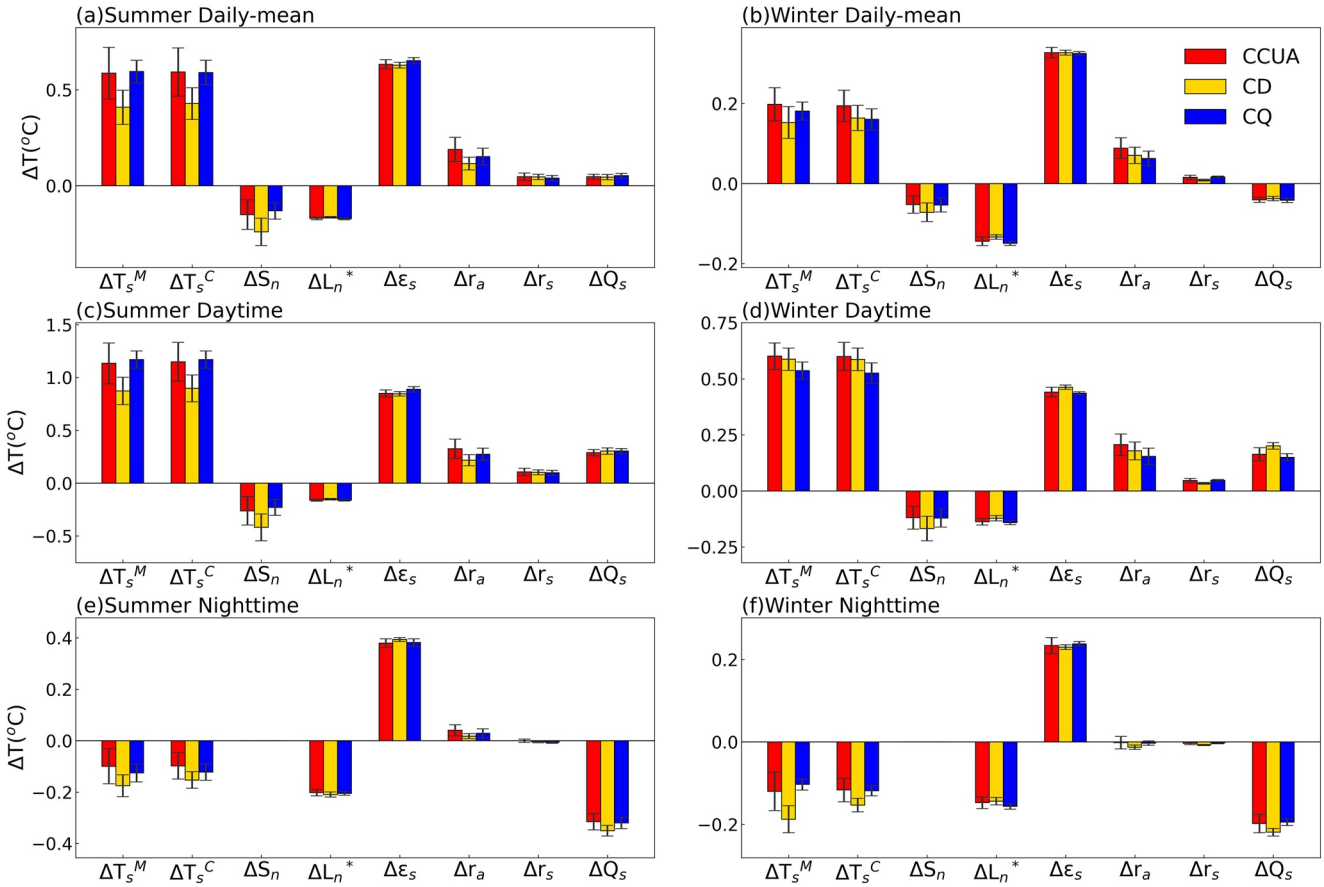

Figure 5. The ΔT_s caused by an increase in the building plan area fraction (lp) and various attributing factors. (a–b) Results of the daily mean in summer and winter. (c–d) Results for the daytime in summer and winter. (e–f) Results for the nighttime in summer and winter. ΔT_s^M and ΔT_s^C represent the simulated ΔT_s and calculated ΔT_s using the summed contributions, respectively, and ΔS_n, ΔL_n^*, $\Delta \varepsilon_s$, Δr_a, Δr_s, and ΔQ_s represent different factors controlling the variations of ΔT_s (see the main text for definitions of these factors). Red, yellow, and blue bars represent results for the Chengdu–Chongqing urban agglomeration (CCUA), Chengdu (CD), and Chongqing (CQ), respectively.

and a negative contribution of ΔQ_s in winter. This is because the increase of the building plan area fraction weakens the effect of heat storage that absorbs heat in summer and releases heat in winter.

During the daytime, a positive ΔT_s is caused by an increase in building plan area fraction, where the related mechanisms are similar to those discussed in the previous paragraph. It is also found that the effect of ΔQ_s is to increase the temperature in both summer and winter (Figures 5c and 5d). This is because the heat storage shows a diurnal pattern of heat absorption during the daytime and heat release during the nighttime. However, during the nighttime, there is a different pattern in ΔT_s (Figures 5e and 5f). Although the warming effect of $\Delta \varepsilon_s$ still provides the largest absolute contribution, the effects of ΔQ_s and ΔL_n provide significant negative contributions, thus counteracting the effect of $\Delta \varepsilon_s$ and cooling the LST at nighttime.

3.2.3. Response of the LST to an Increase of the Average Building Height

Figure 6 has the same layout as the previous figures, and we only discuss the results obtained in the Chengdu–Chongqing urban agglomeration. We can find that an increase of the average building height causes a cooling effect, which contributes ∼−0.27°C in summer and ∼ −0.12°C in winter (Figures 6a and 6b). Among the various considered factors, the effects of Δr_a and $\Delta \varepsilon_s$ are more obvious than the others. According to the study of MacDonald et al. (1998), an increase in the average building height will lead to an increase in the urban roughness. It is also known that increased roughness results in decreased near-surface wind speed and enhanced vertical shear in a horizontal wind, resulting in increased turbulence and convection thermal efficiency (Liu et al., 2017). From the view of land–air interaction, an increase of the roughness will increase the surface exchange coefficient, which will increase the convective heat transfer efficiency, reduce the aerodynamic resistance (r_a; decreasing by

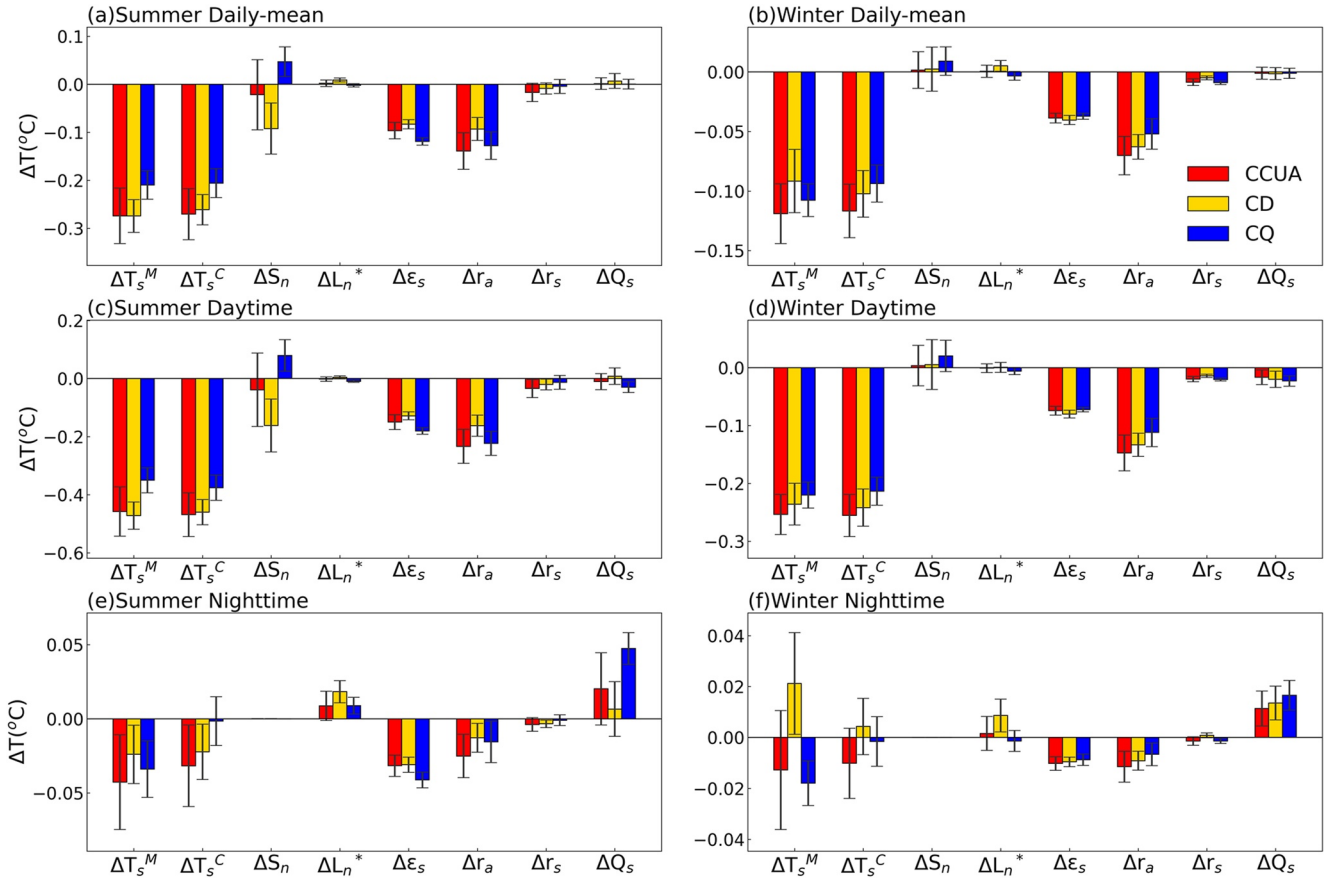

Figure 6. The ΔT_s caused by an increase in the average building height (h) and various attributing factors. (a–b) Results of the daily mean in summer and winter. (c–d) Results for the daytime in summer and winter. (e–f) Results for the nighttime in summer and winter. ΔT_s^M and ΔT_s^C represent the simulated ΔT_s and calculated ΔT_s using the summed contributions, respectively, and ΔS_n, ΔL_n^*, $\Delta \varepsilon_s$, Δr_a, Δr_s, and ΔQ_s represent different factors controlling the variations of ΔT_s (see the main text for definitions of these factors). Red, yellow, and blue bars represent results for the Chengdu–Chongqing urban agglomeration (CCUA), Chengdu (CD), and Chongqing (CQ), respectively.

~0.14°C in summer and ~0.07°C in winter), and finally cause a cooling effect (Chen et al., 1997). The surface exchange coefficient can represent the coupling strength between land and air, and the higher its value, the higher the exchange efficiency of energy and water between land and air. In addition to Δr_a, a larger equivalent surface emissivity (ε_s) also leads to a cooling effect, which contributes ~−0.10°C in summer and ~−0.04°C in winter. We also found that when the average building height changes but the aspect ratio is constant, changes in the capability of the urban surface to capture atmospheric long-wave radiation and solar radiation are little.

During the daytime, ΔT_s caused by an increase in the average building height and the related mechanism is similar to that analyzed in the previous paragraph, where the cooling effect is larger than that for the daily mean (~−0.46°C in summer and ~−0.25°C in winter; Figures 6c and 6d). During the nighttime, the LST changes are very weak, and the consistency between the calculated ΔT_s (ΔT_s^C) and simulated ΔT_s (ΔT_s^M) is poor. This suggests that a change in the average building height has little effect on the nighttime surface temperatures.

4. Conclusions

In this study, we conducted simulations using the WRF model for the Chengdu–Chongqing urban agglomeration in summer and winter to investigate the response of the LST to urban morphological changes, including the aspect ratio, building plan area fraction, and average building height. A method to quantify these contributions was developed based on the TRM method, where we used the equivalent surface emissivity to control the emitted long-wave radiation. We decomposed the changes on the urban LST into contributions from changes in the net solar radiation, atmospheric long-wave radiation absorbed by the surface, equivalent surface emissivity,

aerodynamic resistance, surface resistance, and heat storage in the Chengdu–Chongqing urban agglomeration. The main results and conclusions are as follows.

1. With an increase of the aspect ratio, an increase in the mean LST (~0.13°C) is induced by variations in the net solar radiation (~0.06°C) and absorbed atmospheric long-wave radiation (~0.08°C) in summer. In winter, changes in the absorbed atmospheric long-wave radiation induce a warming effect (~0.05°C). We also found that the daytime cooling and the nighttime warming mainly depend on a change of heat storage (summer: ~−0.52°C during the daytime and ~0.82°C during the nighttime; winter: ~−0.38°C during the daytime and ~0.35°C during the nighttime). In addition, the contributions of differences in the efficiency of the long-wave radiant heat emitted from the surface to the atmosphere are positive during the daytime and negative during the nighttime and the daily mean (summer: ~−0.03°C during the daily mean, ~0.17°C during the daytime and ~−0.36°C during the nighttime).
2. Increasing the building plan area fraction causes the LST to increase (summer: ~0.59°C daily mean; winter: ~0.20°C daily mean). A change in building plan area fraction affects the LST through adjusting the proportion of building areas and street areas. The most obvious factor is a decrease in the efficiency of the long-wave radiant heat emitted from the surface to the atmosphere (summer: ~0.63°C daily mean; winter: ~0.33°C daily mean). In addition, a larger building plan area fraction leads to weakened convective heat transfer and evapotranspiration, and variations in the heat storage provide a positive contribution in summer, a negative contribution in winter, a positive contribution at daytime, and a negative contribution at nighttime. However, during the nighttime, the summed negative contribution of variations in the absorbed atmospheric long-wave radiation and heat storage exceed the positive contribution of the efficiency of the long-wave radiant heat emitted from the surface to the atmosphere, causing a cooling effect.
3. Increasing the average building height causes the LST to decrease (summer: ~−0.27°C daily mean; winter: ~−0.12°C daily mean). Because it increases the surface roughness and enhances the vertical shear of horizontal winds, increased turbulence and convective heat efficiency are produced (summer: ~−0.14°C daily mean; winter: ~−0.07°C daily mean). The contribution of the efficiency of the long-wave radiant heat emitted from the surface to the atmosphere also leads to a cooling effect (summer: ~−0.10°C daily mean; winter: ~−0.04°C daily mean). In addition, when the aspect ratio is constant, changes in the average building height have little effect on the capability of the urban surface to capture solar radiation and atmospheric long-wave radiation.

In general, this study has explored how urban morphological changes affect the LST, which is important for policy makers and planners to formulate urban planning and inform the design of warming mitigation strategies. One limitation of this study and many similar studies about urban LST is neglecting the differences between the different definitions of urban LST. In the single-layer urban canopy model, urban LST is estimated using the Monin–Obukhov similarity theory, and the effects of multiple surfaces (roofs, walls, and streets) are considered. Satellites are advantageous for observing urban LSTs, estimated using long-wave radiation, at spatial scales ranging from neighborhoods to metropolitan regions; however, such data are dominated by street and roof temperatures, with little or no representation of building walls and shaded ground beneath trees. Satellite imagery requires atmospheric or geometric corrections to the LST, and it exhibits temporal and spatial biases arising from clear-sky sampling, fixed and infrequent satellite overpass times, and directional variance in thermal emittance (Stewart et al., 2021); urban LSTs produced by the single-layer urban canopy model are free of these limitations. Moreover, many reanalysis data sets do not distinguish between the definitions of LST in urban areas to natural surfaces, and only regard urban areas as a single surface. These differences bring uncertainties to many studies when verifying simulation results and analyzing urban LST data from different sources.

In addition, it must be recognized that in terms of urban thermal environment characterization, air temperature is more suitable than the LST as the air temperature directly affects human health and well-being. Although air temperature and LST are positively correlated, their spatial patterns and temporal evolution do not completely overlap. Air temperature is more complex than the LST and it can be influenced by more factors in the urban environment, such as wind and airflow, which are linked to air heat transfer that may decouple any consistency between air and surface temperatures (Amani-Beni et al., 2022; Song et al., 2017). Turbulence can effectively enhance the correlation between LST and air temperature, while lower wind speeds can weaken their consistency. LST and air temperature are often close under cloudy or moderate-to-high wind speed conditions or when solar insolation is low or absent. Under cloud-free, low wind speed conditions, the daytime LST is often higher than the air temperature at low-to-middle latitudes (Good, 2016; Good et al., 2017). In this study, we used a method based

on surface energy balance to decompose LST changes into contributions from different physical mechanisms. In the future, our method can be further developed to be applied to air temperature.

Data Availability Statement

The source codes of the WRF Model version 4.1.2 are available at https://www2.mmm.ucar.edu/wrf/users/download/get_source.html [Software] (Skamarock et al., 2019). The NCEP FNL data sets used for WRF simulations were obtained from https://doi.org/10.5065/D6M043C6 [Dataset] (National Centers for Environmental Prediction et al., 2000). The land use and land cover data sets in this work were obtained from https://doi.org/10.12078/2018070201 [Dataset] (Xu et al., 2018). The urban canopy parameters data set of 60 Chinese cities are available at https://doi.org/10.7910/DVN/VZH1QY [Dataset] (Sun et al., 2021), and the FROM-GLC10 data are available at http://data.starcloud.pcl.ac.cn/zh/resource/1 [Dataset] (Gong et al., 2019). The hourly LST product data set of the China Meteorological Administration Land Data Assimilation System (CLDAS) were obtained from http://data.cma.cn/data/cdcdetail/dataCode/NAFP_CLDAS2.0_NRT [Dataset] (Han et al., 2015; Shi et al., 2008, 2011; Sun et al., 2017; Zhu et al., 2013) and the hourly LST product data set of the land component of the fifth generation of European ReAnalysis (ERA5-Land) were obtained from https://doi.org/10.24381/cds.e2161bac [Dataset] (Muñoz Sabater, 2019).

Acknowledgments
We thank the three reviewers and editors for these careful reading and guidance. This work was supported by the National Natural Science Foundation of China (NSFC) project (Grant 41830967), the Strategic Priority Research Program of the Chinese Academy of Sciences (Grant XDA23090102), the National Natural Science Foundation of China (NSFC) project (Grant 42175163, 42205176, and 42205168) and the National Key Scientific and Technological Infrastructure project "Earth System Science Numerical Simulator Facility" (EarthLab).

References

Amani-Beni, M., Chen, Y., Vasileva, M., Zhang, B., & Xie, G. (2022). Quantitative-spatial relationships between air and surface temperature, a proxy for microclimate studies in fine-scale intra-urban areas? *Sustainable Cities and Society*, *77*, 103584. https://doi.org/10.1016/j.scs.2021.103584

Barlage, M., Miao, S., & Chen, F. (2016). Impacts of physical parameterizations on high-resolution weather prediction over two Chinese megacities. *Journal of Geophysical Research: Atmospheres*, *121*, 4487–4498. https://doi.org/10.1002/2015JD024450

Broadbent, A., Krayenhoff, E., & Georgescu, M. (2020). The motley drivers of heat and cold exposure in 21st century US cities. *Proceedings of the National Academy of Sciences of the United States of America*, *117*(35), 21108–21117. https://doi.org/10.1073/pnas.2005492117

Chen, F., & Dudhia, J. (2001). Coupling an advanced land surface–hydrology model with the Penn State–NCAR MM5 modeling system. Part I: Model implementation and sensitivity. *Monthly Weather Review*, *129*(4), 569–585. https://doi.org/10.1175/1520-0493(2001)129<0569:caalsh>2.0.co;2

Chen, F., Janjić, Z., & Mitchell, K. (1997). Impact of atmospheric surface-layer parameterizations in the new land-surface scheme of the NCEP Mesoscale Eta Model. *Boundary-Layer Meteorology*, *85*, 391–421. https://doi.org/10.1023/A:1000531001463

Chen, F., Kusaka, H., Bornstein, R., Ching, J., Grimmond, C. S. B., Grossman-Clarke, S., et al. (2011). The integrated WRF/urban modelling system: Development, evaluation, and applications to urban environmental problems. *International Journal of Climatology*, *31*(2), 273–288. https://doi.org/10.1002/joc.2158

Chen, F., Yang, X., & Zhu, W. (2014). WRF simulations of urban heat island under hot-weather synoptic conditions: The case study of Hangzhou City, China. *Atmospheric Research*, *138*, 364–377. https://doi.org/10.1016/j.atmosres.2013.12.005

Chen, S., Xie, Z., Xie, J., Liu, B., Jia, B., Qin, P., et al. (2022). Impact of urbanization on the thermal environment of the Chengdu–Chongqing urban agglomeration under complex terrain. *Earth System Dynamics*, *13*(1), 341–356. https://doi.org/10.5194/esd-13-341-2022

Dai, Y., Zeng, X., Dickinson, R. E., Baker, I., Bonan, G. B., Bosilovich, M. G., et al. (2003). The common land model. *Bulletin of the American Meteorological Society*, *84*(8), 1013–1024. https://doi.org/10.1175/BAMS-84-8-1013

Deng, X., Cao, Q., Wang, L., Wang, W., Wang, S., & Wang, L. (2022). Understanding the impact of urban expansion and lake shrinkage on summer climate and human thermal comfort in a land-water mosaic area. *Journal of Geophysical Research: Atmospheres*, *127*, e2021JD036131. https://doi.org/10.1029/2021JD036131

Dudhia, J. (1989). Numerical study of convection observed during the winter monsoon experiment using a mesoscale two-dimensional model. *Journal of the Atmospheric Sciences*, *46*(20), 3077–3107. https://doi.org/10.1175/1520-0469(1989)046<3077:NSOCOD>2.0.CO;2

ECMWF. (2018). *IFS documentation cy45r1-part iv: Physical processes*. European Centre for Medium-Range Weather Forecasts (ECMWF). Retrieved from https://www.ecmwf.int/en/elibrary/80895-ifs-documentation-cy45r1-part-iv-physical-processes

Gong, P., Liu, H., Zhang, M., Li, C., Wang, J., Huang, H., et al. (2019). Stable classification with limited sample: Transferring a 30-m resolution sample set collected in 2015 to mapping 10-m resolution global land cover in 2017 [Dataset]. Science Bulletin, *64*, 370–373. https://doi.org/10.1016/j.scib.2019.03.002

Good, E. J. (2016). An in situ-based analysis of the relationship between land surface "skin" and screen-level air temperatures. *Journal of Geophysical Research: Atmospheres*, *121*(15), 8801–8819. https://doi.org/10.1002/2016JD025318

Good, E. J., Ghent, D. J., Bulgin, C. E., & Remedios, J. J. (2017). A spatiotemporal analysis of the relationship between near-surface air temperature and satellite land surface temperatures using 17 years of data from the ATSR series. *Journal of Geophysical Research: Atmospheres*, *122*(17), 9185–9210. https://doi.org/10.1002/2017JD026880

Grimmond, C. S. B., Blackett, M., Best, M. J., Barlow, J., Baik, J.-J., Belcher, S. E., et al. (2010). The international urban energy balance models comparison project: First results from phase 1. *Journal of Applied Meteorology and Climatology*, *49*(6), 1268–1292. https://doi.org/10.1175/2010JAMC2354.1

Grossman-Clarke, S., Zehnder, J. A., Loridan, T., & Grimmond, C. S. B. (2010). Contribution of land use changes to near-surface air temperatures during recent summer extreme heat events in the Phoenix metropolitan area. *Journal of Applied Meteorology and Climatology*, *49*(8), 1649–1664. https://doi.org/10.1175/2010JAMC2362.1

Guo, G., Zhou, X., Wu, Z., Xiao, R., & Chen, Y. (2016). Characterizing the impact of urban morphology heterogeneity on land surface temperature in Guangzhou, China. *Environmental Modelling and Software*, *84*, 427–439. https://doi.org/10.1016/j.envsoft.2016.06.021

Han, S., Shi, C., Lin, H., Meng, X., & Lu, H. (2015). The CLDAS soil moisture operation products applied to monitor soil drought [Dataset]. Journal of Glaciology and Geocryology, *37*, 446–453. Retrieved from https://kns.cnki.net/kcms2/article/abstract?v=mFW-2yKNQdpw-d_-Anx-

hsTU4oPPoNxuUO88mAderklc4jOIIhGT8wqrn0FxoTp5e39oq-EznApNYCRT_XZ-NDNxH-a8y35pcQdf0Sj0c6_JCfH8BkdWlsfPlG63Ng-9HupXUW_RVdLHM=&uniplatform=NZKPT&language=CHS

Hang, J., & Chen, G. (2022). Experimental study of urban microclimate on scaled street canyons with various aspect ratios. *Urban Climate*, *46*, 101299. https://doi.org/10.1016/j.uclim.2022.101299

Hong, S.-Y., Noh, Y., & Dudhia, J. (2006). A new vertical diffusion package with an explicit treatment of entrainment processes. *Monthly Weather Review*, *134*(9), 2318–2341. https://doi.org/10.1175/mwr3199.1

Huang, K., Lee, X., Stone, B., Jr., Knievel, J., Bell, M. L., & Seto, K. C. (2021). Persistent increases in nighttime heat stress from urban expansion despite heat island mitigation. *Journal of Geophysical Research: Atmospheres*, *126*(4), e2020JD033831. https://doi.org/10.1029/2020JD033831

Jiménez, P. A., Dudhia, J., González-Rouco, J. F., Navarro, J., Montávez, J. P., & García-Bustamante, E. (2012). A revised scheme for the WRF surface layer formulation. *Monthly Weather Review*, *140*(3), 898–918. https://doi.org/10.1175/MWR-D-11-00056.1

Kain, J. S. (2004). The Kain–Fritsch convective parameterization: An update. *Journal of Applied Meteorology and Climatology*, *43*(1), 170–181. https://doi.org/10.1175/1520-0450(2004)043<0170:TKCPAU>2.0.CO;2

Kanda, M., Kanega, M., Kawai, T., Moriwaki, R., & Sugawara, H. (2007). Roughness lengths for momentum and heat derived from outdoor urban scale models. *Journal of Applied Meteorology and Climatology*, *46*(7), 1067–1079. https://doi.org/10.1175/JAM2500.1

Khan, A., Khorat, S., Doan, Q.-V., Khatun, R., Das, D., Hamdi, R., et al. (2023). Exploring the meteorological impacts of surface and rooftop heat mitigation strategies over a tropical city. *Journal of Geophysical Research: Atmospheres*, *128*(8), e2022JD038099. https://doi.org/10.1029/2022JD038099

Kim, G., Cha, D.-H., Song, C.-K., & Kim, H. (2021). Impacts of anthropogenic heat and building height on urban precipitation over the Seoul metropolitan area in regional climate modeling. *Journal of Geophysical Research: Atmospheres*, *126*, e2021JD035348. https://doi.org/10.1029/2021JD035348

Krayenhoff, E., Moustaoui, M., Broadbent, A., Gupta, V., & Georgescu, M. (2018). Diurnal interaction between urban expansion, climate change and adaptation in US cities. *Nature Climate Change*, *8*(12), 1097–1103. https://doi.org/10.1038/s41558-018-0320-9

Kusaka, H., Chen, F., Bao, J., Tewari, M., & Hirakuchi, H. (2004). Simulation of the urban heat island effects over the Greater Houston Area with the high resolution WRF/LSM/Urban coupled system. *Simulation*, *1*, 4. https://ams.confex.com/ams/pdfpapers/70370.pdf

Kusaka, H., & Kimura, F. (2004). Coupling a single-layer urban canopy model with a simple atmospheric model: Impact on urban heat island simulation for an idealized case. *Journal of the Meteorological Society of Japan. Series II*, *82*(1), 67–80. https://doi.org/10.2151/jmsj.82.67

Kusaka, H., Kondo, H., Kikegawa, Y., & Kimura, F. (2001). A simple single-layer urban canopy model for atmospheric models: Comparison with multi-layer and slab models. *Boundary-Layer Meteorology*, *101*, 329–358. https://doi.org/10.1023/A:1019207923078

Lai, D., Liu, W., Gan, T., Liu, K., & Chen, Q. (2019). A review of mitigating strategies to improve the thermal environment and thermal comfort in urban outdoor spaces. *Science of the Total Environment*, *661*, 337–353. https://doi.org/10.1016/j.scitotenv.2019.01.062

Lai, S., Zhao, Y., Fan, Y., & Ge, J. (2021). Characteristics of daytime land surface temperature in wind corridor: A case study of a hot summer and warm winter city. *Journal of Building Engineering*, *44*, 103370. https://doi.org/10.1016/j.jobe.2021.103370

Lan, Y., & Zhan, Q. (2017). How do urban buildings impact summer air temperature? The effects of building configurations in space and time. *Building and Environment*, *125*, 88–98. https://doi.org/10.1016/j.buildenv.2017.08.046

Li, C., Lu, H., Yang, K., Wright, J. S., Yu, L., Chen, Y., et al. (2017). Evaluation of the common land model (CoLM) from the perspective of water and energy budget simulation: Towards inclusion in CMIP6. *Atmosphere*, *8*(8), 141. https://doi.org/10.3390/atmos8080141

Li, C., & Zhang, N. (2021). Analysis of the daytime urban heat island mechanism in east China. *Journal of Geophysical Research: Atmospheres*, *126*, e2020JD034066. https://doi.org/10.1029/2020JD034066

Li, D., Bou-Zeid, E., Baeck, M. L., Jessup, S., & Smith, J. A. (2013). Modeling land surface processes and heavy rainfall in urban environments: Sensitivity to urban surface representations. *Journal of Hydrometeorology*, *14*(4), 1098–1118. https://doi.org/10.1175/JHM-D-12-0154.1

Li, Y., Schubert, S., Kropp, J. P., & Rybski, D. (2020a). On the influence of density and morphology on the Urban Heat Island intensity. *Nature Communications*, *11*, 2647. https://doi.org/10.1038/s41467-020-16461-9

Li, Z., Zhang, H., Wen, C. Y., Yang, A. S., & Juan, Y. H. (2020b). Effects of frontal area density on outdoor thermal comfort and air quality. *Building and Environment*, *180*, 107028. https://doi.org/10.1016/j.buildenv.2020.107028

Liao, W., Liu, X., Burakowski, E., Wang, D., Wang, L., & Li, D. (2020). Sensitivities and responses of land surface temperature to deforestation-induced biophysical changes in two global earth system models. *Journal of Climate*, *33*(19), 8381–8399. https://doi.org/10.1175/JCLI-D-19-0725.1

Liao, W., Rigden, A., & Li, D. (2018). Attribution of local temperature response to deforestation. *Journal of Geophysical Research: Biogeosciences*, *123*(5), 1572–1587. https://doi.org/10.1029/2018JG004401

Liu, R., Han, Z., Wu, J., Hu, Y., & Li, J. (2017). The impacts of urban surface characteristics on radiation balance and meteorological variables in the boundary layer around Beijing in summertime. *Atmospheric Research*, *197*, 167–176. https://doi.org/10.1016/j.atmosres.2017.07.006

Macdonald, R. W., Griffiths, R. F., & Hall, D. J. (1998). An improved method for the estimation of surface roughness of obstacle arrays. *Atmospheric Environment*, *32*(11), 1857–1864. https://doi.org/10.1016/S1352-2310(97)00403-2

Marciotto, E. R., Oliveira, A. P., & Hanna, S. R. (2010). Modeling study of the aspect ratio influence on urban canopy energy fluxes with a modified wall-canyon energy budget scheme. *Building and Environment*, *45*(11), 2497–2505. https://doi.org/10.1016/j.buildenv.2010.05.012

Millstein, D., & Menon, S. (2011). Regional climate consequences of large-scale cool roof and photovoltaic array deployment. *Environmental Research Letters*, *6*(3), 034001. https://doi.org/10.1088/1748-9326/6/3/034001

Mlawer, E. J., Taubman, S. J., Brown, P. D., Iacono, M. J., & Clough, S. A. (1997). Radiative transfer for inhomogeneous atmospheres: RRTM, a validated correlated-k model for the longwave. *Journal of Geophysical Research*, *102*(D14), 16663–16682. https://doi.org/10.1029/97JD00237

Mohammed, A., Khan, A., & Santamouris, M. (2021). On the mitigation potential and climatic impact of modified urban albedo on a subtropical desert city. *Building and Environment*, *206*, 108276. https://doi.org/10.1016/j.buildenv.2021.108276

Monaghan, A. J., Hu, L., Brunsell, N. A., Barlage, M., & Wilhelmi, O. V. (2014). Evaluating the impact of urban morphology configurations on the accuracy of urban canopy model temperature simulations with MODIS. *Journal of Geophysical Research: Atmospheres*, *119*, 6376–6392. https://doi.org/10.1002/2013JD021227

Muñoz Sabater, J. (2019). ERA5-Land hourly data from 1950 to present [Dataset]. Copernicus Climate Change Service (C3S) Climate Data Store (CDS). https://doi.org/10.24381/cds.e2161bac

National Centers for Environmental Prediction/National Weather Service/NOAA/U.S. Department of Commerce. (2000). NCEP FNL operational model global tropospheric analyses, continuing from july 1999 [Dataset]. Research Data Archive at the National Center for Atmospheric Research, Computational and Information Systems Laboratory. https://doi.org/10.5065/D6M043C6

Nazarian, N., & Kleissl, J. (2015). CFD simulation of an idealized urban environment: Thermal effects of geometrical characteristics and surface materials. *Urban Climate*, *12*, 141–159. https://doi.org/10.1016/j.uclim.2015.03.002

Niu, G.-Y., Yang, Z.-L., Mitchell, K. E., Chen, F., Ek, M. B., Barlage, M., et al. (2011). The community noah land surface model with multiparameterization options (Noah-MP): 1. Model description and evaluation with local-scale measurements. *Journal of Geophysical Research*, *116*, D12109. https://doi.org/10.1029/2010JD015139

Oleson, K. W., Niu, G.-Y., Yang, Z.-L., Lawrence, D. M., Thornton, P. E., Lawrence, P. J., et al. (2007). *CLM3.5 documentation*. Community Land Model 3.5 Public Release Home Page. Retrieved from https://www2.cgd.ucar.edu/tss/clm/distribution/clm3.5/CLM3_5_documentation.pdf

Peng, J., Xie, P., Liu, Y., & Ma, J. (2016). Urban thermal environment dynamics and associated landscape pattern factors: A case study in the Beijing metropolitan region. *Remote Sensing of Environment*, *173*, 145–155. https://doi.org/10.1016/j.rse.2015.11.027

Rigden, A. J., & Li, D. (2017). Attribution of surface temperature anomalies induced by land use and land cover changes. *Geophysical Research Letters*, *44*, 6814–6822. https://doi.org/10.1002/2017GL073811

Rigo, G., & Parlow, E. (2007). Modelling the ground heat flux of an urban area using remote sensing data. *Theoretical and Applied Climatology*, *90*(3), 185–199. https://doi.org/10.1007/s00704-006-0279-8

Salamanca, F., Martilli, A., Tewari, M., & Chen, F. (2011). A study of the urban boundary layer using different urban parameterizations and high-resolution urban canopy parameters with WRF. *Journal of Applied Meteorology and Climatology*, *50*(5), 1107–1128. https://doi.org/10.1175/2010JAMC2538.1

Salamanca, F., Zhang, Y., Barlage, M., Chen, F., Mahalov, A., & Miao, S. (2018). Evaluation of the WRF-urban modeling system coupled to Noah and Noah-MP land surface models over a semiarid urban environment. *Journal of Geophysical Research: Atmospheres*, *123*, 2387–2408. https://doi.org/10.1002/2018JD028377

Sharma, A., Fernando, H. J. S., Hamlet, A. F., Hellmann, J. J., Barlage, M., & Chen, F. (2016). Urban meteorological modeling using WRF: A sensitivity study. *International Journal of Climatology*, *37*, 1885–1900. https://doi.org/10.1002/joc.4819

Shi, C., Xie, Z., Qian, H., Liang, M., & Yang, X. (2011). China land soil moisture EnKF data assimilation based on satellite remote sensing data [Dataset]. Science China Earth Sciences, *54*, 1430–1440. https://doi.org/10.1007/s11430-010-4160-3

Shi, C., Xie, Z., Tian, X., Qian, H., & Liang, M. (2008). Research on satellite remote sensing soil moisture assimilation based on EnKF algorithm [Dataset]. Collected Papers on Satellite Remote Sensing Application Technology and Processing Methods at the 2008 Annual Meeting of the Chinese Meteorological Society, *372*. Retrieved from https://kns.cnki.net/kcms2/article/abstract?v=3uoqIhG8C467SBiOvrai6cVePIGuwmb-S3U2ptMn63qTfswhRKNQyoX_bDv8X720vKZnhbzJZNl5vZbapQsZd6C6lxNj0VPkr&uniplatform=NZKPT

Skamarock, C., Klemp, B., Dudhia, J., Gill, O., Liu, Z., Berner, J., et al. (2019). A description of the advanced research WRF model version 4.1 [Software]. UCAR/NCAR - Library. https://doi.org/10.5065/1dfh-6p97

Song, J., Wang, Z.-H., Myint, S. W., & Wang, C. (2017). The hysteresis effect on surface-air temperature relationship and its implications to urban planning: An examination in Phoenix, Arizona, USA. *Landscape and Urban Planning*, *167*, 198–211. https://doi.org/10.1016/j.landurbplan.2017.06.024

Stewart, I. D., Krayenhoff, E. S., Voogt, J. A., Lachapelle, J. A., Allen, M. A., & Broadbent, A. M. (2021). Time evolution of the surface urban heat island. *Earth's Future*, *9*(10), e2021EF002178. https://doi.org/10.1029/2021EF002178

Stewart, I. D., & Oke, T. R. (2012). Local climate zones for urban temperature studies. *Bulletin of the American Meteorological Society*, *93*(12), 1879–1900. https://doi.org/10.1175/BAMS-D-11-00019.1

Sun, S., Shi, C., Liang, X., Han, S., Jiang, Z., & Zhang, T. (2017). Assessment of ground temperature simulation in China by different land surface models based on station observations [Dataset]. Journal of Applied Meteorological Science, *28*, 737–749. https://doi.org/10.11898/1001-7313.20170609

Sun, Y., Zhang, N., Miao, S., Kong, F., Zhang, Y., & Li, N. (2021). Urban morphological parameters of the main cities in China and their application in the WRF model [Dataset]. Journal of Advances in Modeling Earth Systems, *13*. e2020MS002382. https://doi.org/10.1029/2020MS002382

Susca, T., Gaffin, S. R., & Dell'Osso, G. (2011). Positive effects of vegetation: Urban heat island and green roofs. *Environmental Pollution*, *159*(8–9), 2119–2126. https://doi.org/10.1016/j.envpol.2011.03.007

Thompson, G., Field, P. R., Rasmussen, R. M., & Hall, W. D. (2008). Explicit forecasts of winter precipitation using an improved bulk microphysics scheme. Part II: Implementation of a new snow parameterization. *Monthly Weather Review*, *136*(12), 5095–5115. https://doi.org/10.1175/2008MWR2387.1

United Nations. (2019). *World urbanization prospects: The 2018 revision*. Department of Economic and Social Affairs, Population Division.

Wang, X., Hui, E., Choguill, C., & Jia, S. (2015). The new urbanization policy in China: Which way forward? *Habitat International*, *47*, 279–284. https://doi.org/10.1016/j.habitatint.2015.02.001

Wang, X., Liu, H., Miao, S., Wu, Q., Zhang, N., & Qiao, F. (2020). Effectiveness of urban hydrological processes in mitigating urban heat island and human thermal stress during a heat wave event in Nanjing, China. *Journal of Geophysical Research: Atmospheres*, *125*, e2020JD033275. https://doi.org/10.1029/2020JD033275

Xu, X., Liu, J., Zhang, S., Li, R., Yan, C., & Wu, S. (2018). China's multi-period land use land cover remote sensing monitoring data set (CNLUCC) [Dataset]. Resource and Environment Data Cloud Platform. https://doi.org/10.12078/2018070201

Yang, J., Jin, S., Xiao, X., Jin, C., Xia (Cecilia), J., Li, X., & Wang, S. (2019). Local climate zone ventilation and urban land surface temperatures: Towards a performance-based and wind-sensitive planning proposal in megacities. *Sustainable Cities and Society*, *47*, 101487. https://doi.org/10.1016/j.scs.2019.101487

Yang, J., Yang, Y., Sun, D., Jin, C., & Xiao, X. (2021). Influence of urban morphological characteristics on thermal environment. *Sustainable Cities and Society*, *72*, 103045. https://doi.org/10.1016/j.scs.2021.103045

Yang, X., & Li, Y. (2015). The impact of building density and building height heterogeneity on average urban albedo and street surface temperature. *Building and Environment*, *90*, 146–156. https://doi.org/10.1016/j.buildenv.2015.03.037

Yang, X., Li, Y., Luo, Z., & Chan, P. W. (2017). The urban cool island phenomenon in a high-rise high-density city and its mechanisms. *International Journal of Climatology*, *37*, 890–904. https://doi.org/10.1002/joc.4747

Zhou, R., Jiang, W., He, X., & Liu, G. (2009). Study on effects of building morphology on urban boundary layer using an urban canopy model. *Journal of Meteorological Research*, *23*(3), 338–349. Retrieved from http://jmr.cmsjournal.net/article/id/1193

Zhou, Y., Smith, S. J., Zhao, K., Imhoff, M., Thomson, A., Bond-Lamberty, B., et al. (2015). A global map of urban extent from nightlights. *Environmental Research Letters*, *10*(5), 054011. https://doi.org/10.1088/1748-9326/10/5/054011

Zhu, C., Shi, C., Celine, & Huang, X. (2013). Simulation and evaluation of soil moisture at different depths in the Chinese region [Dataset]. Meteorological Science and Technology, *41*, 529–536. https://doi.org/10.19517/j.1671-6345.2013.03.019